ChemElectroChem

Research Article
doi.org/10.1002/celc.202300208

Chemistry Europe
European Chemical Societies Publishing

www.chemelectrochem.org

Investigation of Multi-Phase Structure and Optoelectronic Performance of Bi-Doped (Cu–Zn) Oxide Composite Thin Films

Yasemin Altinay,[a] Abdullah Akkaya,[b] Rasit Aydin,[c] and Bünyamin Sahin*[d]

In this research, thin film composite structures were used to prepare optoelectronic devices from bare and Bi-substituted p-CuO/n-ZnO systems. The p-CuO/n-ZnO composite thin film structures were prepared by the SILAR technique, and the influences of two different Bi contents on the structure and main physical performances of the samples were investigated. The X-ray diffraction (XRD) technique showed that the composited thin film materials were multiphased in rutile hexagonal (wurtzite) phase (ZnO) and monoclinic tenorite phase (CuO) type crystal structure. The obtained surface morphological results presented that the structure exhibits an almost homogeneous, plate-like surface distribution, and depending on the increase of Bi concentration, the plate-like sheet area widens from ~2.5 μm to 10 μm and the layer boundaries decrease. FT-IR and Raman spectroscopy were used to investigate the various vibration and Raman active phonon modes of Bi:p-CuO/n-ZnO nanostructured heterostructures. For a comprehensive analysis of the optical bandgap of the fabricated composite samples, the estimated values were obtained from the Tauc plot. Produced samples exhibited an Ohmic behavior and dc resistivity values of films can be determined via Ohm's Law. The adjusted sheet resistance value of 11.51 MΩ/sq when the content of Bi 3.0% in the growth bath.

Introduction

Composite structures are obtained by combining two or more materials with different physical and chemical properties. Nanocomposite (NC) materials, especially nanostructured metal oxide (MO) materials, have an important place in the production and use of nanomaterials. NC structures have different properties with the materials that make them up. These structures, unlike alloys and mixtures, do not dissolve in each other. This makes it possible to obtain materials with different properties.[1] NC structures consisting of two or more different materials can show different behaviors in the morphological, structural, optical, electrical, and mechanical analysis due to being both nanostructure and composite material. This provides an increase in the diversity of producing new materials.[2] The advantages of nanocomposite materials are that they are cheap, light, and long lasting, have high physical and chemical resistance, and most importantly, they can be produced in different combinations.[3] Thin films obtained from NC materials attract great attention due to their excellent optical, electrical, mechanical, and tribological characteristics as well as their wide range of applications. These films are widely used in the chemical, automotive, aerospace, biomedical, and electronics industries due to their interesting properties such as great resistance to oxidation and corrosion at high temperatures, and high hardness. In addition, NC materials are used in various industries such as sports, defense, and architectural sectors due to their flexibility in design and lightweight.[4]

Common stoichiometric copper oxides, cuprous oxide, Cu_2O ("red"), and cupric oxide, CuO ("black"), were well-known materials for semiconductor devices and photoelectric and/or photoconductive applications, respectively.[5] Cupric oxide (CuO) is also a semiconductor, which has an indirect band gap and is smaller than cuprous oxide. Both copper oxides show a p-type semiconductor behavior caused by metal deficiency (copper vacancy generation).[5,6] Similarly, zinc oxide (ZnO) is chemically stable and has a wide and direct band gap.[7] Unlike copper oxides, ZnO shows an n-type semiconductor behavior, which is caused by the oxygen vacancies in the crystal structure.[7a,8] When the literature is examined, it is seen that zinc oxide (ZnO) and copper oxide (CuO) MOs are widely used

[a] Dr. Y. Altinay
Technology and Research & Development Center (MARGEM)
Hatay Mustafa Kemal University
31400 Hatay (Turkey)

[b] Dr. A. Akkaya
Mucur Technical Vocational Schools
Tech. Prog. Department
Kırşehir Ahi Evran University
40500 Kırşehir (Turkey)

[c] Dr. R. Aydin
Department of Physics
Faculty of Sciences
Selçuk University
42130 Konya (Turkey)

[d] Prof. B. Sahin
Department of Basic Sciences
Faculty of Engineering
Necmettin Erbakan University
42140 Konya (Turkey)
E-mail: bunyamin.sahin@erbakan.edu.tr
Homepage: http://www.erbakan.edu.tr/en/personel/14322/bunyamin-sahin

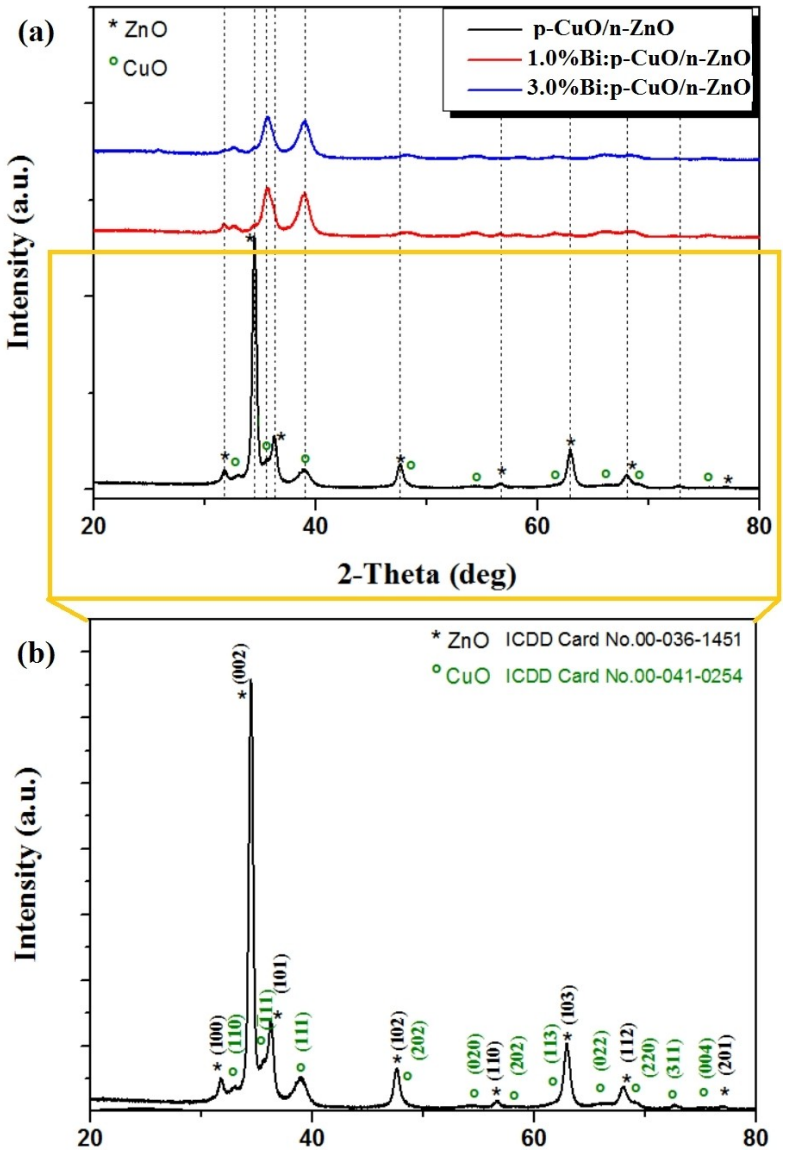

Figure 1. (a) X-ray diffraction patterns of the synthesized bare and Bi-substituted p-CuO/n-ZnO composite films. (b) The XRD pattern shown with the orange rectangular part is indexed with the ICDD Card No. 00-036-1451 and ICDD Card No. 00-041-0254 for hexagonal wurtzite ZnO and monoclinic CuO, respectively.

Table 1. The calculated average crystallite size, relative peak intensity and FWHM values of bare and Bi-substituted p-CuO/n-ZnO thin films.

Sample Name	Relative Peak Intensity (a.u.)		FWHM		Crystallite size [nm]
	CuO (111)	ZnO (100)	CuO (111)	ZnO (100)	
p-CuO/n-ZnO	455	365	1.130	0.52	12.91
1.0% Bi: p-CuO/n-ZnO	1403	196	1.178	1.40	7.06
3.0% Bi: p-CuO/n-ZnO	1200	209	1.291	1.24	7.20

Table 2. Sheet resistance (R_S) values of bare and Bi-substituted p-CuO/n-ZnO thin films as a function of Bi content.

Sample Name	ϱ [x10^8 Ω]	t [nm]	R_S [×10^7 Ω/sq.]
p-CuO/n-ZnO	3.291	447.9	7.347
1.0% Bi: p-CuO/n-ZnO	1.422	550.4	2.584
3.0% Bi: p-CuO/n-ZnO	0.820	712.2	1.151

in the production of NC structures. Since these two metal oxides are both abundant and frequently used in many technological fields, the properties of composite structures consisting of them attract the attention of researchers.[9] Among these MOs, the non-toxic ZnO material is wurtzite-structured oxide, due to its properties such as a large band gap (3.36 eV), n-type semi-conductivity, beautiful optical transparency (> 80%), wide exciton binding energy (60 meV).[10] Another metal oxide material, CuO, has advantages such as non-toxicity, p-

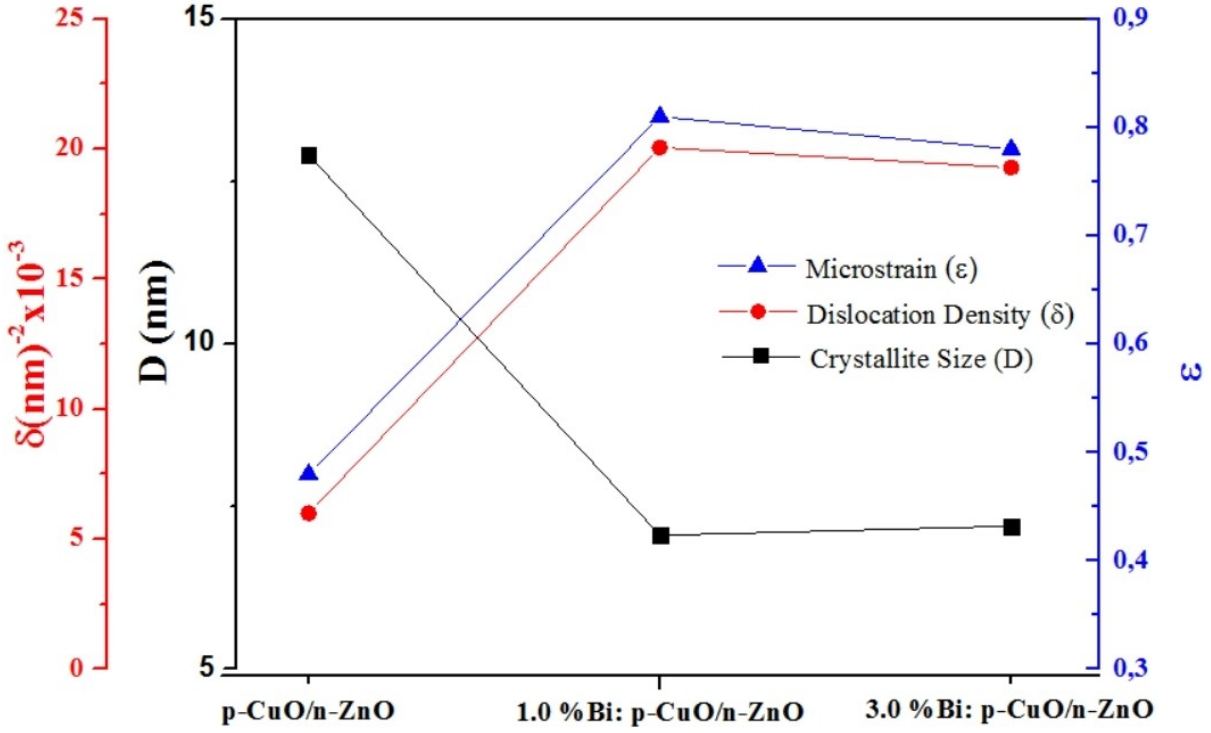

Figure 2. The variations in average crystallite size, dislocation density and microstrain of the synthesized bare and Bi-substituted p-CuO/n-ZnO nanostructured films.

type semi-conductivity, high absorption coefficient, and adjustable band gap (1.2–1.9 eV).[11]

Due to their superior properties, p-CuO/n-ZnO NC thin film structures are used in many applications such as gas detection, solar cells, glucose sensors, UV absorbers, photo catalysts, and chemical sensors.[12] p-CuO/n-ZnO NCs have been synthesized using many techniques such as sputtering, sol-gel, chemical vapor synthesis, pulsed laser deposition, molecular beam epitaxy, and successive ionic layer adsorption and reaction (SILAR).[13] Among these methods, SILAR is a promising technique as it is relatively simple, environmentally friendly, safe, low-temperature compatible, and cost-effective.[14]

Various methods are used to improve the physical performance of nanostructured p-CuO/n-ZnO thin films. One of these methods is doping. The doping technique is a technique that can be used both to control the structural, morphological, optical, and electrical properties of nanostructured MO semiconductors and to obtain new multifunctional semiconductor materials. Many doping elements such as Er, Al, Mn, Fe, N, Na, and K were used by researchers to increase the main physical and chemical properties of materials.[15] The effect of different concentrations of these doping elements on physical and chemical properties has become a focus for many researchers.

Among these doping elements, Bismuth (Bi) is a non-magnetic atom. The Bi dopant is non-ferri- or ferromagnetic in its bulk form. In particular, Bi has been used as an additive in catalytic applications. The oxide state of Bi, Bi_2O_3, is an important MO semiconductor with a wide energy range (2–3.98 eV). Bi_2O_3 is used in supercapacitor applications due to its excellent redox behavior and high energy density. Additionally, Bi_2O_3 is a good solid electrolyte material used in ceramic glass production and optical coatings due to its high oxygen ion conductivity.[16]

Therefore, in this study, Bi-substituted p-CuO/n-ZnO composite films, which have remarkable physical and chemical properties, can be effective in solution-based reactions and are frequently used in the development of structural, morphological, and optical properties, were synthesized by the SILAR method. Three different p-CuO/n-ZnO films were produced depending on different concentrations of Bi (0.0%, 1.0%, and 3.0%, respectively). The effects of Bi concentration ratios on the structural, morphological, optical, and electrical properties of the synthesized p-CuO/n-ZnO films were investigated.

Results and Discussions

The X-ray diffraction technique was used to provide insight into the crystallographic nature (crystalline structure, average crystallite size, dislocation density, microstrain, etc.) of the p-CuO/n-ZnO nanostructured films. Figure 1 shows the XRD patterns of p-CuO/n-ZnO, 1.0% Bi:p-CuO/n-ZnO, and 3.0% Bi:p-CuO/n-ZnO nanostructured films and CuO and ZnO with ICDD card no. of bare p-CuO/n-ZnO films, respectively.

XRD results showed that bare and Bi-substituted p-CuO/n-ZnO films were successfully synthesized by the SILAR technique. As it is observed from Figure 1, the diffraction peaks of ZnO show the hexagonal (wurtzite) phase with P63mc (ICDD card

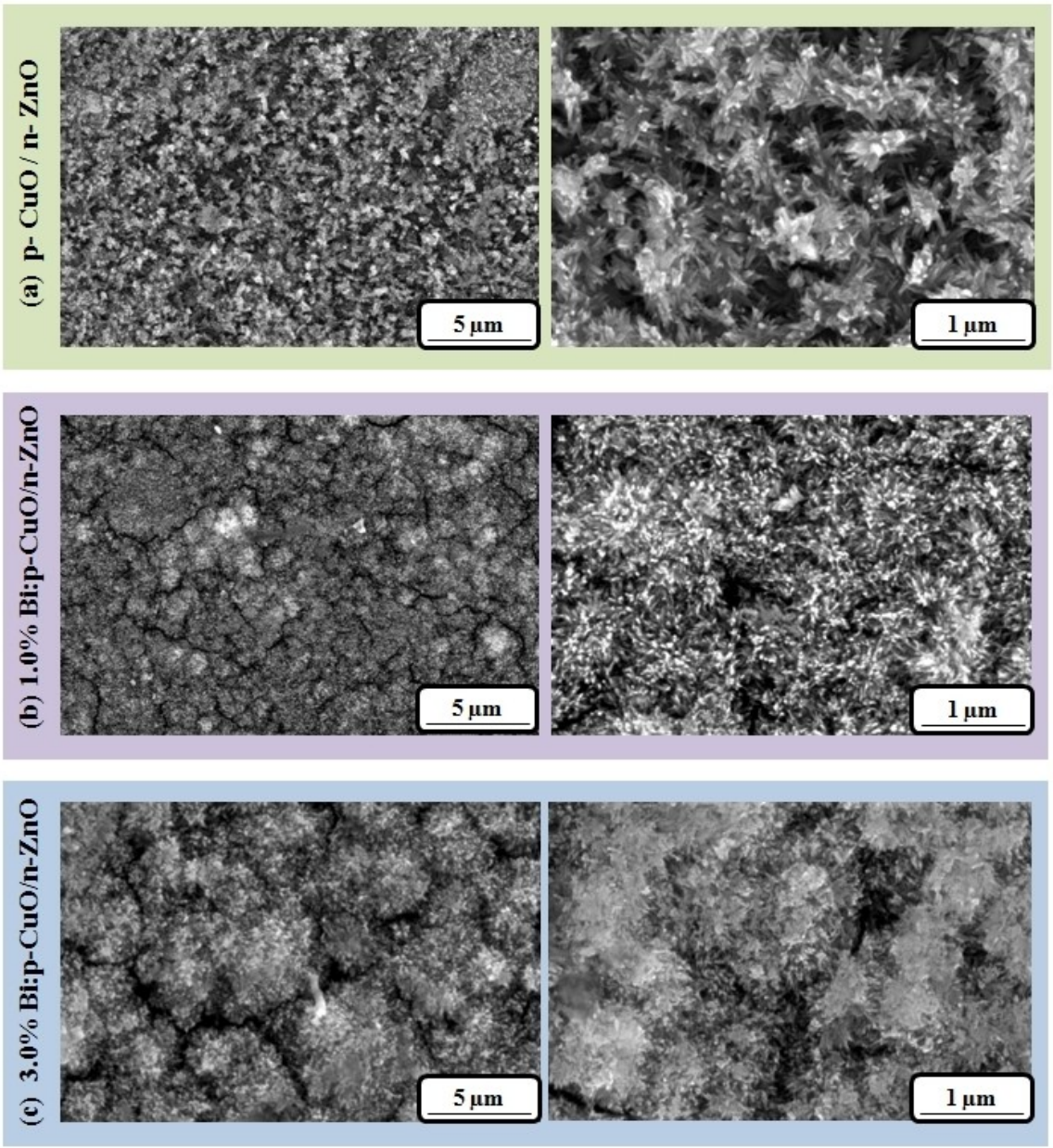

Figure 3. SEM images of **(a)** p-CuO/n-ZnO, **(b)** 1.0% Bi:p-CuO/n-ZnO and **(c)** 3.0% Bi:p-CuO/n-ZnO nanostructured films at different magnifications. It is seen that the granular nanostructures are aggregated with the Bi additive ratio and clustered as a micro-sponge structure to form plate-like layers.

No. 00-036-1451), while the diffraction peaks of CuO show the monoclinic tenorite phase with 15: C12/c1 (ICDD card No. 00-041-0254). Moreover, no extra characteristic phases were detected in the XRD pattern of the films. The average crystallite size (D) of the films was calculated using the Scherrer equation (Eq. 1);

$$D = \frac{0.94\lambda}{\beta cos\theta} \quad (1)$$

where λ is the wavelength of the X-ray radiation (1.5406 Å), β represents the FWHM (full width half maximum) of the peak related to 2θ and θ is the diffraction angle.[17]

In addition to the grain morphologic properties of the nanostructured films, the dislocation density and microstrain parameters are important parameters that determine the microstructure. When the lattice constants are not matched in structures, chemical bonds occur at the hetero-interface, and this causes the formation of crystalline dislocations and structure defects as it creates microstrain in the structure. Therefore, dislocation morphology plays a major role in determining the microstructural properties of films. Dislocation density, δ is a function of average crystallite size from the XRD pattern (Eq. 2);[18]

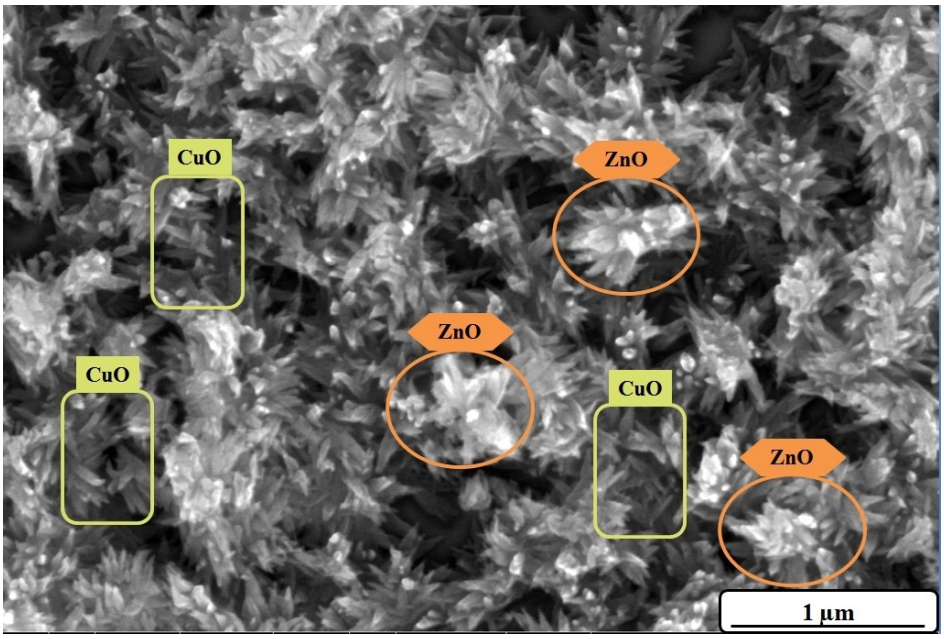

Figure 4. SEM images of the bare p-CuO/n-ZnO nanostructured film. Similarly, ZnO and CuO nanoparticles have been determined and demonstrated in the previous literature as a result of SEM-EDX.[50]

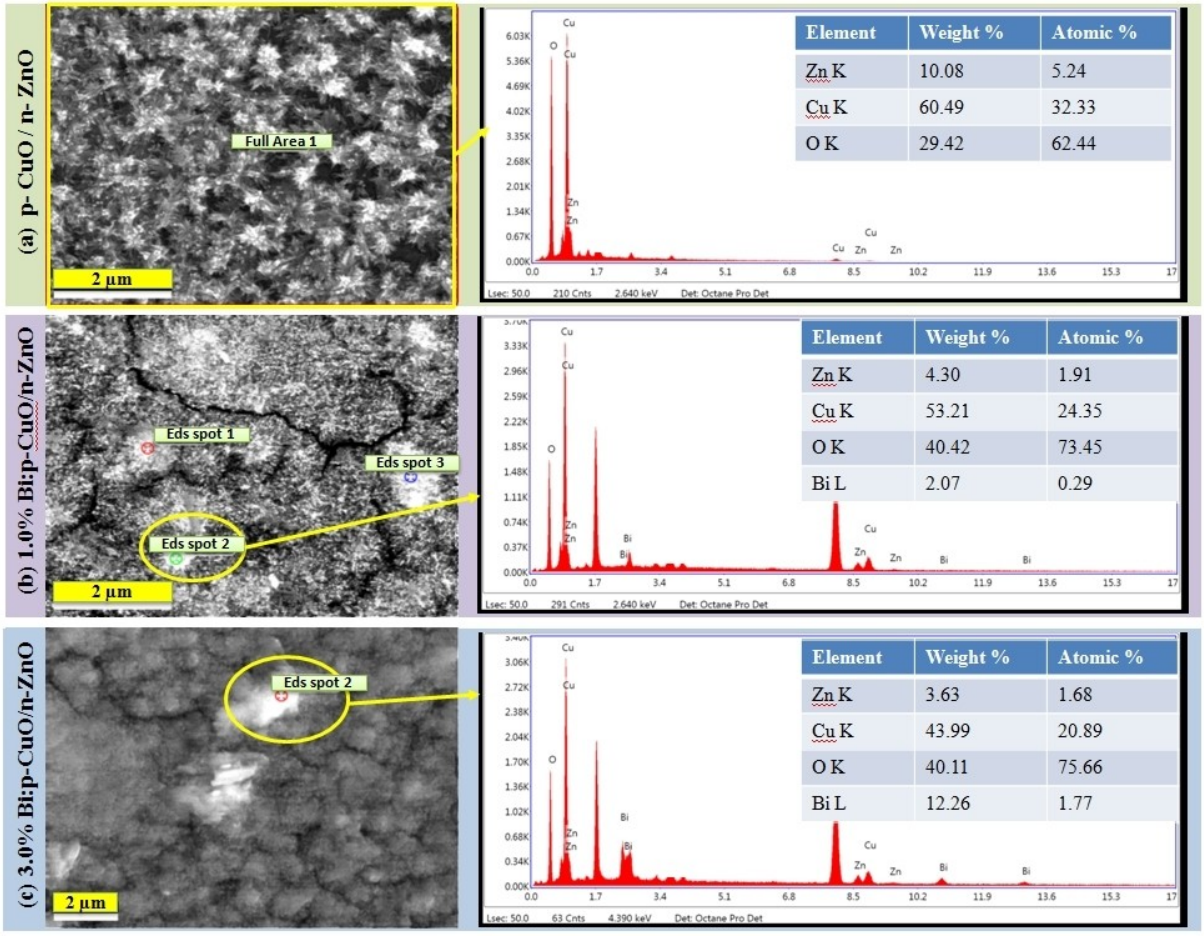

Figure 5. SEM-EDX analysis results of **(a)** p-CuO/n-ZnO, **(b)** 1.0% Bi:p-CuO/n-ZnO and **(c)** 3.0% Bi:p-CuO/n-ZnO nanostructured films. The presence of Bi element was observed in Bi-substituted p-CuO/n-ZnO film. Considering the weight and atomic percentage values in the elemental analysis, it is seen that Cu and O are more dominant than Zn and Bi in the films.

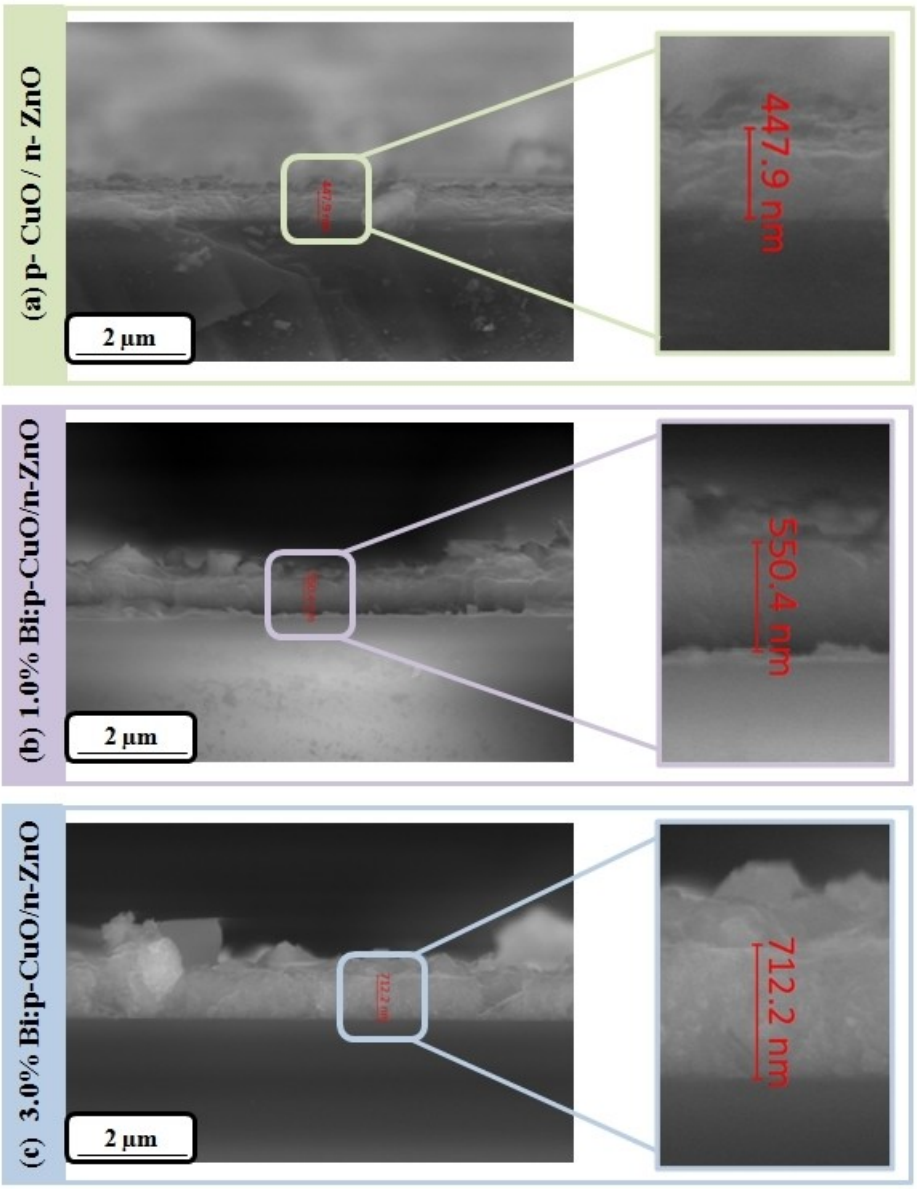

Figure 6. Cross-sectional SEM images (with 50000x magnification and 2 µm resolution) of (a) p-CuO/n-ZnO, (b) 1.0% Bi:p-CuO/n-ZnO and (c) 3.0% Bi:p-CuO/n-ZnO nanocomposite films. It can be seen that thin film thickness increased with Bi additive ratio.

$$\delta = \frac{1}{D^2} \tag{2}$$

The degree of distortion in the crystallite lattice of the structure is expressed as a microstrain. Both the average crystallite size and microstrain in the crystallite lattice effect of the line broadening (FWHM) in the X-ray diffraction pattern. Therefore, determining the microstrain of the structure is important for the crystallography of films of different orientations. The microstrain, ε is given in the following equation (Eq. 3);[18a,19]

$$\varepsilon = \frac{\beta}{4tan\theta} \tag{3}$$

The calculated average crystallite size, relative peak intensity and FWHM values of p-CuO/n-ZnO films are shown in Table 1.

As observed in Table 1 that the relative peak intensity of the ZnO (002) peak position, and the corresponding FWHM values were destroyed by the deposition of Bi^{5+} in the p-CuO/n-ZnO film. This is also clearly seen in the XRD pattern given in Figure 1. Kumar et al., was stated that the addition of Bi to the p-CuO/n-ZnO nanostructured films caused a significant decrease in the ZnO (002) diffraction peak.[20] Additionally, the relative peak intensity of the ZnO (100) peak position decreased with the increase of Bi concentrations, while the relative peak intensity of the CuO (111) peak position increased significantly. Therefore, it can be said that with the addition of Bi to the p-CuO/n-ZnO film the Bi^{5+} ions penetrate the CuO and ZnO lattice plane and the CuO lattice is dominant compared to ZnO

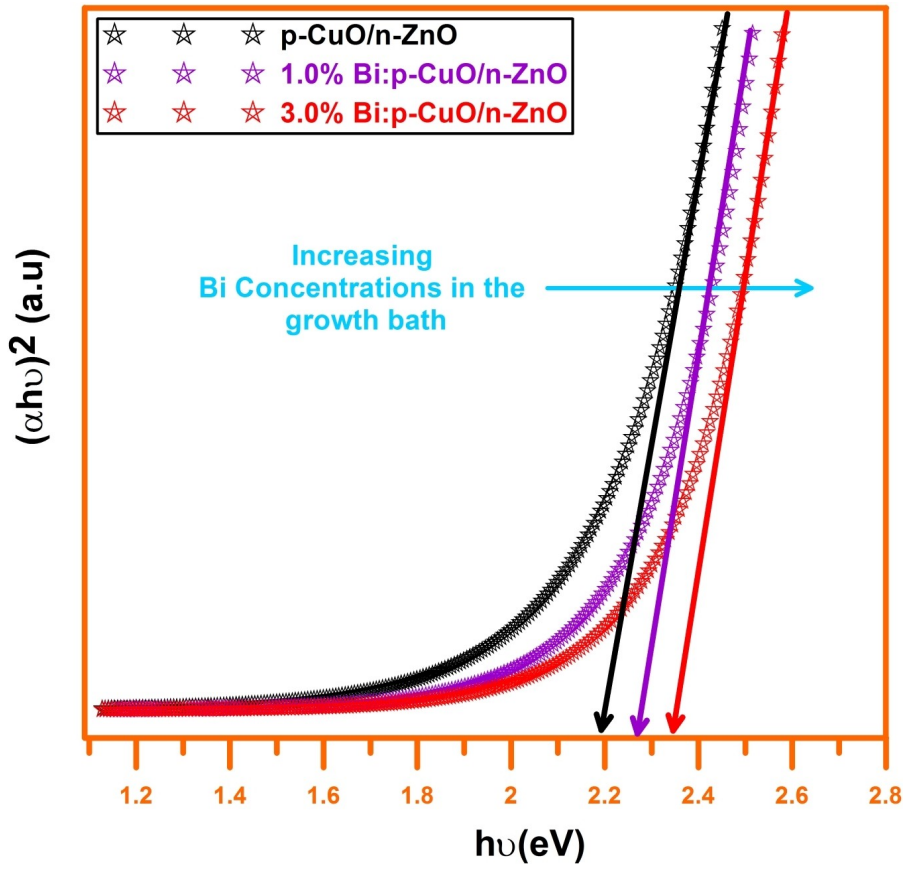

Figure 7. Tauc plots for the estimation of bandgap energy of the Bi:p-CuO/n-ZnO nanocomposite thin films. The E_g value was calculated as 2.20 eV for the bare p-CuO/n-ZnO film. The E_g values of the Bi-doped p-CuO/n-ZnO films were found to be 2.27 (1.0% Bi) and 2.35 eV (3.0% Bi), respectively. Since the E_g of Bi_2O_3 (in the range of about 2.4-3.96 eV) is larger than that of p-CuO/n-ZnO (2.20 for current work), the E_g of Bi-doped p-CuO/n-ZnO should be larger than that of bare p-CuO/n-ZnO.

lattice in the structure. Depending on the obvious increase in FWHM values for the CuO (111) plane and decrease in FWHM values for the ZnO (002) and (100) planes, the crystallite size values of the films decreased from 12.91 nm to 7.20 nm. The crystallite size was increased from 7.06 nm to 7.20 nm with increasing Bi concentration. An increase in the crystallite size with the addition of Bi to ZnO and CuO has also been specified in similar studies in the literature.[21]

The variation between crystallite size, dislocation density and microstrain of the p-CuO/n-ZnO films is graphed in Figure 2.

It can be seen from Figure 2, dislocation density and microstrain values exhibit an inverse behavior with the average crystallite size calculations. This is due to the decrease in defect levels and grain boundaries with increasing average crystallite size. This behavior was also observed in similar literature studies.[19b,22]

The morphological structure of the films was investigated using SEM analysis. Figure 3 indicates the SEM images of bare and Bi-substituted p-CuO/n-ZnO nanostructured films synthesized by the SILAR method at different resolutions and magnifications. As can be seen in Figure 3 and Figure 4.

The bare p-CuO/n-ZnO film is a mixture of leaf-like CuO and flower-like ZnO nanostructures (about 250–500 nm in diameter).[23] Additionally, due to the accumulation of CuO and ZnO on the surface, a voided and irregular structure was observed in places (Figure 4). By adding Bi to the p-CuO/n-ZnO film, it was observed that at lower magnifications (20000x magnification, 5 μm resolution), nano-flower and nano-leaf-shaped structures clustered as one of the micro-sponge structure and formed a plate-like layer. The micro-sponge structures were even more uniformly arranged at higher magnification (100000× magnification, 1 μm resolution) with larger plate-like sheet sizes formed by tightly packed nano-structures. Therefore, it is seen that the structure exhibits an almost homogeneous, plate-like surface distribution, and depending on the increase of Bi concentration, the plate-like sheet area widens from ~2.5 μm to 10 μm and the layer boundaries decrease. This situation is a result observed in other studies in the literature[24] and is consistent with the XRD analysis.

The EDX mapping and associated elemental analysis are given in Figure 5. As shown in Figure 5, the presence of zinc (Zn), copper (Cu) and oxygen (O) elements were detected in the bare p-CuO/n-ZnO film. In addition to these elements, the presence of Bi element was observed in Bi-substituted p-CuO/n-ZnO film.

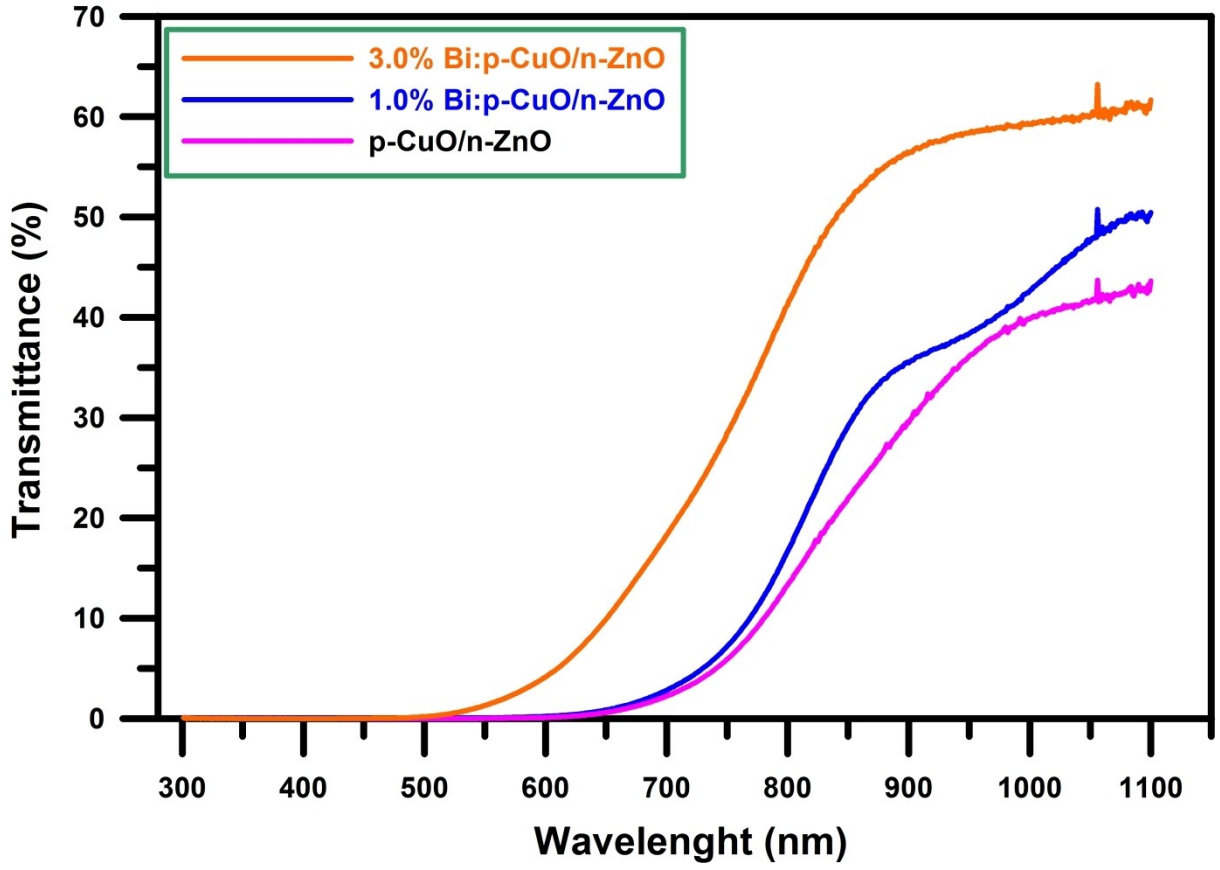

Figure 8. Transmittance spectra of the of the Bi:p-CuO/n-ZnO nanocomposite thin films. The bare p-CuO/n-ZnO film has 43% transmittance at high wavelengths (~1100 nm). With the increase of Bi content, the transmittance of Bi-doped p-CuO/n-ZnO films increased from 50% (1.0% Bi: p-CuO/n-ZnO) to 62% (3.0% Bi: p-CuO/n-ZnO), respectively.

Considering the weight and atomic percentage values in the elemental analysis, it is seen that Cu and O are more dominant than Zn and Bi in the films. It was observed that the Bi peak intensity and elemental composition increased in structure with increasing Bi concentration. All SEM-EDX analysis results showed good agreement with XRD analysis. The cross-sectional SEM images (with 50000x magnification and 2 μm resolution) of bare and Bi-substituted p-CuO/n-ZnO nanostructured films are presented in Figure 6. Figure 6 showed that the thin film thickness increased from 447.9 nm to 712.2 nm with increasing Bi content in the growth bath. Since the difference in the atomic radius of the dopants affects the nucleation rate of the crystal structure, it significantly changes the surface morphology (particle distribution) of the material and thus the film thickness. The large difference in the Bi atomic radius (230 p.m.) compared to Cu (145 p.m.) and Zn (142 p.m.) changed the nucleation rate, especially because of the size and distribution change.[15e]

UV-Vis. the spectrometer was used to determine the optical band gap energies (E_g) of bare p-CuO/n-ZnO and Bi-doped p-CuO/n-ZnO films. The E_g values of these films were calculated using the Tauc equation (Eq. 4).[25]

$$\alpha h\nu = C(h\nu - E_g)^{1/2} \quad (4)$$

In this equation, $h\nu$, and α correspond to the incident photon energy and absorption coefficient, respectively. Starting from this, the graphs of change of $(\alpha h\nu)^2$ versus photon energy $(h\nu)$ of all produced p-CuO/n-ZnO films are given in Figure 7. The tangent lines drawn to the horizontal axis in the graph correspond to the E_g values. The E_g value was calculated as 2.20 eV for the bare p-CuO/n-ZnO film.

This result is in agreement with the results previously found in the literature.[26] The E_g values of the Bi-doped p-CuO/n-ZnO films were found to be 2.27 (1.0% Bi) and 2.35 eV (3.0% Bi), respectively. Since the E_g of Bi_2O_3 (in the range of about 2.4-3.96 eV) is larger than that of p-CuO/n-ZnO (2.20 for current work), the E_g of Bi-doped p-CuO/n-ZnO should be larger than that of bare p-CuO/n-ZnO.[27] Additionally, this increase in E_g values (blue shift) may be due to states filled with electrons (Burstein-Moss effect) pushing the Fermi level to higher energy in the conduction band.[28]

Optical transmittance curves of bare and Bi-doped p-CuO/n-ZnO films in the range of 300–1200 nm wavelengths are shown in Figure 8. The bare p-CuO/n-ZnO film has 43% transmittance at high wavelengths (~1100 nm). With the increase of Bi content, the transmittance of Bi-doped p-CuO/n-ZnO films increased from 50% (1.0% Bi: p-CuO/n-ZnO) to 62% (3.0% Bi:

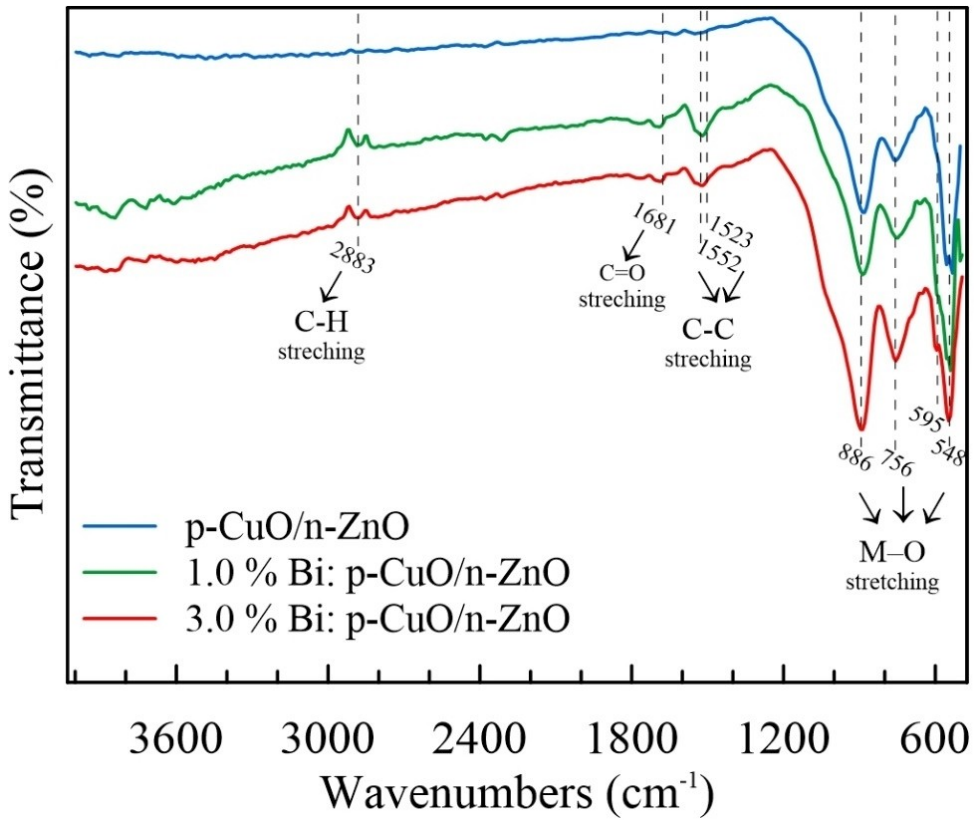

Figure 9. FTIR spectrum of bare and Bi-substituted p-CuO/n-ZnO nanocomposite thin films. ZnO and CuO both exhibit absorption bands in the fingerprint region (i.e., below 1000 cm^{-1}) due to their stretching modes as in metal-oxide materials.

p-CuO/n-ZnO), respectively. The augment in transmittance can be associated with a well-crystal structure, which wanes the scattering of light.[29] Additionally, crystal defects and crystal size from multiple oxide materials in the film can alter the transparency.[30]

Raman and FT-IR spectroscopy were used to investigate the various vibration and Raman active phonon modes of bare and Bi-substituted p-CuO/n-ZnO nanostructured heterostructure. Figure 9 exhibits the FTIR spectrum of the bare and Bi-substituted p-CuO/n-ZnO samples obtained in the range of 400–4000 cm^{-1}.

ZnO and CuO both exhibit absorption bands in the fingerprint region (i.e., below 1000 cm^{-1}) due to their stretching modes as in metal-oxide materials. Four strong peaks appeared at 548, 595, 756, and 886 cm^{-1} can be assigned to the overlapped of the typical stretching mode of the Cu–O and Zn–O bonds.[1b,31] These results confirm the obtained structure of the nanoscale composite and supported decent with the XRD results. On the other hand, no considerable shifts in the peaks were noticed owing to the implementation of Bi to ZnO–CuO heterostructure. This affirms that there is no chemical bond consists between ZnO, CuO and Bi, as noticed in the XRD results. In addition, a few vibration modes were observed in the rest of the FTIR spectrum of Bi substituted CuO–ZnO films. These peaks can be ascribed to the residual precursors and organic contamination.[31a]

Figure 10 shows the Raman spectra of bare and Bi-substituted p-CuO/n-ZnO heterostructure thin films. Along with the vibrations of wurtzite ZnO, monoclinic CuO has been observed for bare and Bi-substituted p-CuO/n-ZnO heterostructure. The co-presence of CuO and ZnO Raman modes in the Raman spectra affirms the creation of p-CuO/n-ZnO heterostructure. As we know from group theory, CuO in the monoclinic crystal structure has 12 ($4A_u+5B_u+A_g+2B_g$) and ZnO in the wurtzite structure has 6 ($A_1+2B_1+E_1+2E_2$) symmetry modes.[32] For CuO, only three of these modes are Raman active modes and are denoted in the spectrum at A_g (289 cm^{-1}), B_{1g} (339 cm^{-1}), and B_{2g} (618 cm^{-1}), which correspond to vibration of oxygen atoms only.[33] For ZnO, A_1 and E_1 modes are both infrared and Raman active but they polarized in different directions (polar mode) and split the polar modes into longitudinal optical (LO) and transverse optical (TO) components.[34] In addition, two B_1 modes (high and low), which arise from the sub-lattice oscillations, are silent and two E_2 modes (high and low) are non-polar and only Raman active.[34,35]

The polar A_1 (LO) (571 cm^{-1}) vibrational mode corresponds to the vibration of Zn and O atoms in a rigid sublattice. The peak at around 1106 cm^{-1} corresponds to second-order Raman scattering of the A_1 (LO) mode of ZnO, which was observed in bare and Bi-substituted p-CuO/n-ZnO thin film spectrums.[33b,35b,36] E_2 vibrational modes (E_2 (low) and E_2 (high)) are nonpolar due to mutual cancelation of the displacement vectors of the individual sublattice. On the other hand, this

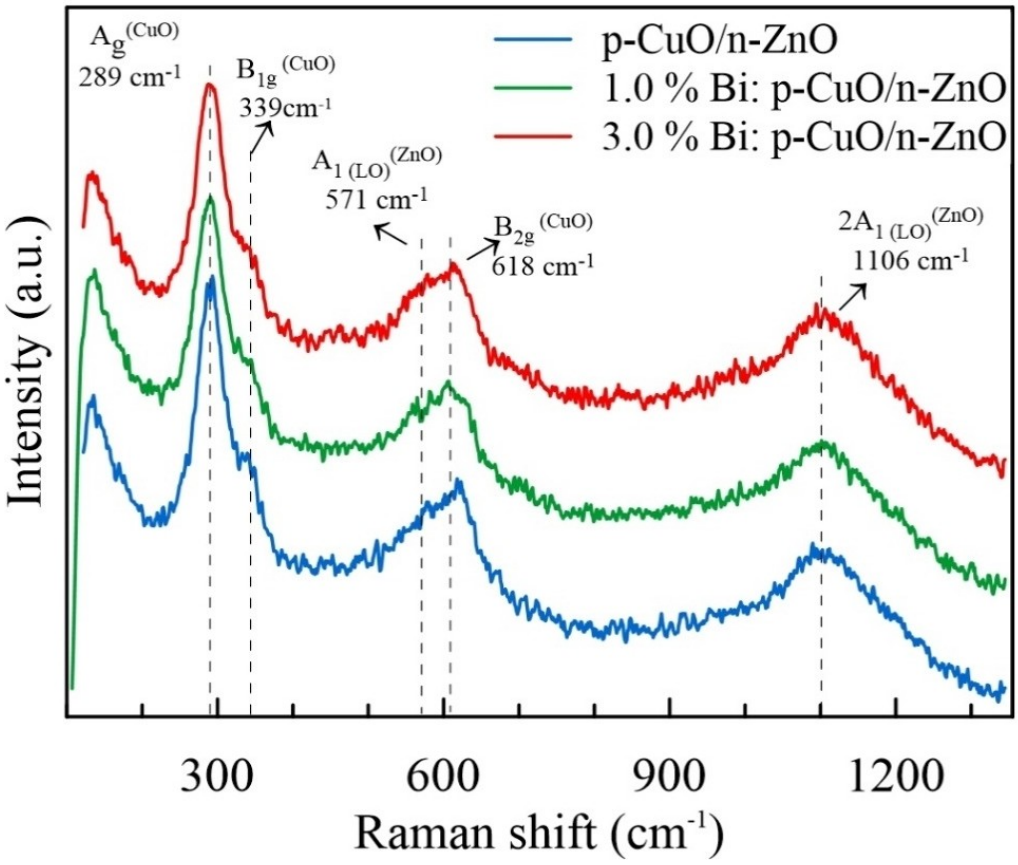

Figure 10. Raman spectra of p-CuO/n-ZnO nanocomposite samples with different content of Bi doping using the 515 nm excitation. Dashed lines as an eye guide.

peaks not observed in the spectrum, possibly these peaks could be restriction of the corresponding vibrational modes in the nanocomposite structures.[33b] Moreover, A_1 (LO) and E_1 (LO) frequencies of the Raman modes were also shown in the finger print region of the IR spectrum (see on lowest frequency region in Figure 9).

As can be seen in Figure 10, the positions of peaks are almost constant for bare and Bi -substituted thin films and there is no peak observed for another related to the Bi-based compound. Furthermore, intensity variations and broadening or redshift in Raman peaks were not also observed, which can be easily associated with slight lattice disorder with Bi doping. So, Bi has been successfully doped into the host CuO/ZnO matrix at cationic sites.

Figure 11 shows current-voltage (I-V) measurement results of bare and Bi-substituted p-CuO/n-ZnO films within the range of −5 to 5 V at room temperature. Films exhibited an Ohmic behavior and dc resistivity values of films can be determined via Ohm's Law *(R = V/I)*, but, these resistivity values cannot define the dc resistivity characteristics of films because of their own nature. In situations like this, sheet resistivity values of samples were calculated using the equation, as given below (Eq. 5);[13e,37]

$$R_s = \rho/t \tag{5}$$

where ρ and t were the resistivity and thickness of the deposited bare and Bi-substituted p-CuO/n-ZnO films, respectively.

According to Table 2, the dc resistivity values decreased with the Bi content. This case was generally interconnect with the change in grain boundaries or scattering phenomenon of dopant electrons due to the considerable doping content and ionized electrons.[1b,38] Here, the doping ratio was low; however, the change in some parameters (e.g. decrease in crystallite size and increase in thickness) with increasing Bi doping rate is remarkable. (See Tables 1 and 2). So, this significant drop in sheet resistance can be elucidated by the not only film parameters, but also existence of dopant atoms, which act as superficial acceptors in ZnO-CuO matrices.[1b,31a,38,39] These dopant atoms act as superficial acceptors in ZnO-CuO and reason reduced hole content and scattering of holes at the native defects corresponding to higher mobility and lower resistance.[31a]

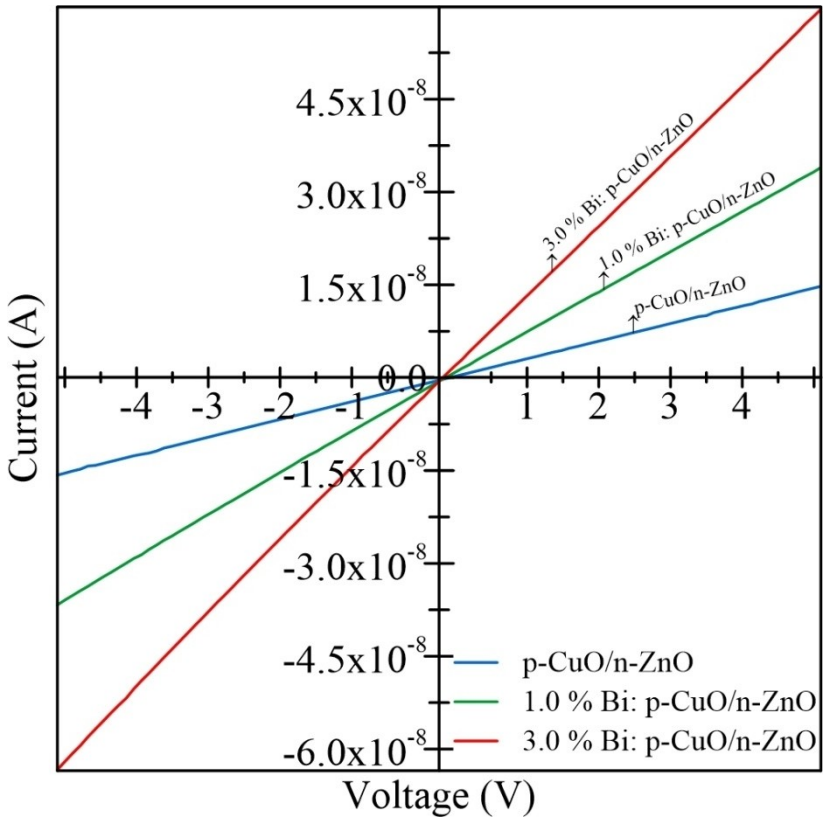

Figure 11. I–V characteristics of the Bi-substituted p-CuO/n-ZnO films. The dc resistivity values decreased with the Bi content. This case was generally interconnect with the change in grain boundaries or scattering phenomenon of dopant electrons due to the considerable doping content and ionized electrons.

Conclusions

Bare and Bi-substituted p-CuO/n-ZnO composite films were synthesized by SILAR technique, a low cost and simple technique and the structural, morphological, optical, and electrical properties of these films were studied. XRD analysis confirmed that all p-CuO/n-ZnO films obtained were polycrystalline in nature and the crystallite size varied from 12.91 nm to 7.06 nm. It can be seen from the SEM images that the bare p-CuO/n-ZnO film is a mixture of leaf-like CuO and flower-like ZnO nanostructures. EDX elemental analysis supports the presence of Cu, Zn, O and Bi in the composition. FTIR and Raman spectra confirmed Zn–O and Cu–O vibrational bands and ZnO and CuO Raman modes, respectively. It was found from UV-vis analysis that as the Bi-doping concentration increases, the E_g (from 2.20 to 2.35 nm) and optical transmission (from 43% to 62%) values increased. It was found that the R_s decreased from 7.347 to 1.151 ($\times 10^7$ Ω/sq.) with Bi doping. From the results obtained, it is thought that Bi-substituted p-CuO/n-ZnO composite films will contribute to various new technological and optoelectronic applications.

Experimental Details

Different cationic precursors such as zinc acetate dihydrate, copper (II) chloride dihydrate, and bismuth(III) chloride are used to synthesize p-CuO/n-ZnO, 1.0% Bi:p-CuO/n-ZnO and 3.0% Bi:p-CuO/n-ZnO films by the SILAR technique. In a typical synthesis, first, aqueous solutions containing 50 ml 0.1 M Copper (II) chloride dehydrate ($CuCl_2.2H_2O$) and 50 ml 0.1 M Zinc acetate dihydrate ($Zn(CH_3COO)_2 \cdot 2H_2O$) reagents were used in the of p-CuO/n-ZnO nanostructured films. The reagents were stirred for a few minutes at room temperature in a magnetic stirrer to obtain a homogeneous growth bath. Ammonium hydroxide and NH_4OH were added to optimize the pH ($\sim 10.00 \pm 0.05$) of the growth bath and then SILAR solution was heated at 85 °C at 300 rpm. For depositing p-CuO/n-ZnO nanostructured films, the pre-cleaned substrates were immersed in a precursor solution for 20 s, as shown in Figure 12.

Zinc and copper ions adsorbed on the surface of the substrates and then substrates were rinsed in deionized water (85 °C, 300 rpm for 20 s). This SILAR synthesis process was repeated 20 times to acquire good quality p-CuO/n-ZnO thin films. The basic reaction equations for the formation of CuO thin films on glass slides by SILAR method are as follows (Eqs. 6–7):[40]

$$CuCl_2 + 6NH_4OH \rightarrow [Cu(NH_3)_4]^{+2} + 2OH^- + 4H_2O + 2NH_4Cl \quad (6)$$

$$[Cu(NH_3)_4]^{+2} + 3H_2O \rightarrow CuO + 4NH_4{}^+ + 2OH^- \quad (7)$$

Similarly, the basic reactions for the formation of ZnO thin films are as follows (Eqs. 8–9):[41]

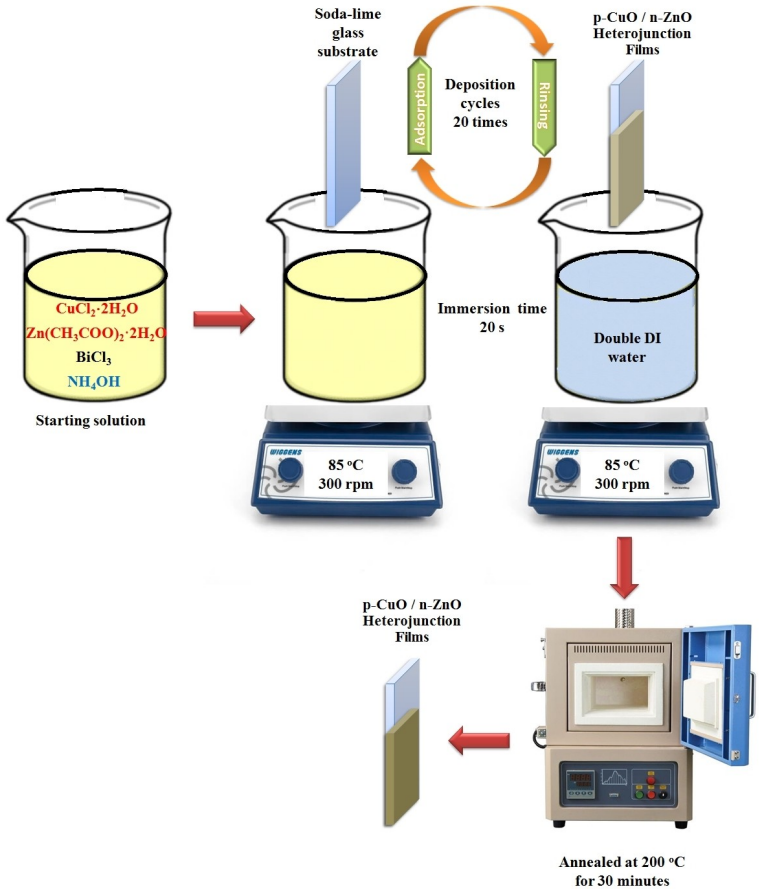

Figure 12. The schematic diagram of the SILAR technique for deposition of bare and Bi-substituted p-CuO/n-ZnO composite films.

$$Zn(CH_3COO)_2 + 2NH_4OH \rightarrow Zn(OH)_2 + 2CH_3COONH_4 \quad (8)$$

$$Zn(OH)_2 \rightarrow ZnO + H_2O \quad (9)$$

1.0% Bi:p-CuO/n-ZnO and 3.0% Bi:p-CuO/n-ZnO nanostructured films were synthesized by the same SILAR procedure to investigate the effect of Bi^{5+} (1.0% and 3.0%) on the nanostructured films. Finally, all the nanostructured films were at 200 °C for 30 min in ambient air.[1b,42]

The p-CuO/n-ZnO nanostructured films were characterized by X-ray diffraction (XRD), scanning electron microscopy (SEM), ultraviolet visible (UV-Vis.) spectrometer, Fourier transform infrared (FT-IR), micro Raman spectrometer, and electrical resistivity measurement methods. XRD patterns of the thin films have been performed with the aid of Rigaku SmartLab (40 keV, 30 mA) in the scan range from 20° to 80° (2 theta) and scan rate 2°/min using Cu Kα radiation ($\lambda =$ 1.5406 Å). The scanning electron microscope (SEM; FEI QUANTA FEG 250) was used to characterize the surface morphological properties of the films. The energy dispersive X-ray spectroscopy (EDX; FEI QUANTA ESEM FEG 250) was determined by elemental composition analysis of the films. The optical transmittance and absorption spectra of the films were registered using a Thermo Scientific Genesys 10S UV-Vis. spectrometer. A Shimadzu IRAffinity-1S Fourier transform infrared (FT-IR) spectroscopy (spectral range 4000 cm^{-1}–400 cm^{-1}, with ATR method) was used to determine the chemical bonding structure or functional groups of films. The inVia Renishaw micro-Raman spectrometer (532 nm) was used in the range of 100–1200 cm^{-1} to investigate the microstructural nature of films. The electrical resistivity measurement was carried out using a Keithley 6487 picoammeter/voltage source at 300 K temperature.

Acknowledgements

This study was supported by TÜBİTAK ULAKBİM (The Scientific and Technological Research Council of Turkey) Read & Publish Program.

Conflict of Interests

The authors declare no conflict of interest.

Data Availability Statement

The data that support the findings of this study are available from the corresponding author upon reasonable request.

Keywords: Band gap · CuO · nanocomposite · resistivity · ZnO

[1] a) M. Marzuki, N. M. Rusdi, M. Z. M. Zain, M. Izaki, *J. Sol-Gel Sci. Technol.* **2021**, *100*, 388–403; b) O. Kahveci, A. Akkaya, E. Yücel, R. Aydın, B. Şahin, *Ceram. Int.* **2023**, *49*, 16458–16466; c) B. Pal, B. L. Vijayan, S. G. Krishnan, M. Harilal, W. J. Basirun, A. Lowe, M. M. Yusoff, R. Jose, *J. Alloys Compd.* **2018**, *740*, 703–710; d) M. Batool, R. Gill, K. Munawar, V. McKee, M. Mazhar, *J. Solid State Chem.* **2022**, *305*, 122642.
[2] a) M.-X. Nie, X.-Z. Li, S.-R. Liu, Y. Guo, *Sens. Actuators B* **2015**, *210*, 211–217; b) M. Pandey, M. Singh, K. Wasnik, S. Gupta, S. Patra, P. S. Gupta, D. Pareek, N. S. N. Chaitanya, S. Maity, A. B. M. Reddy, R. Tilak, P. Paik, *ACS Omega* **2021**, *6*, 31615–31631.
[3] a) G. Soni, N. Gouttam, P. Soni, *Mater. Today: Proc.* **2020**, *30*, 35–38; b) M. S. Abdel-wahab, A. R. Wassel, A. H. Hammad, *J. Electron. Mater.* **2020**, *49*, 7179–7186.
[4] a) E. A. Sharma, *Nanocomposite Materials for Biomedical and Energy Storage Applications*, IntechOpen, Rijeka, **2022**, p. 340; b) M. Thariq, V. R. Kar, S. K. Panda, K. Jayakrishna, *Advanced Composite Materials and Structures: Modeling and Analysis*, CRC Press, Boca Raton, **2023**, p. 308.
[5] C. G. Ribbing, A. Roos, in *Handbook of Optical Constants of Solids* (Ed.: E. D. Palik), Academic Press, Burlington, **1997**, pp. 875–882.
[6] A. R. Carrasco-Hernández, R. I. Ruvalcaba-Ontiveros, E. Martínez-Guerra, J. A. Duarte-Moller, H. E. Esparza-Ponce, *J. Nanomater.* **2022**, *2022*, 7964428.
[7] a) B. Nirmala, T. V. Banumathi, M. Najeema, M. Kayalvizhi, *Asian J. Chem.* **2013**, *25*, S103-S106; b) M. Kahouli, A. Barhoumi, A. Bouzid, A. Al-Hajry, S. Guermazi, *Superlattices Microstruct.* **2015**, *85*, 7–23.
[8] a) L. Liu, Z. Mei, A. Tang, A. Azarov, A. Kuznetsov, Q.-K. Xue, X. Du, *Phys. Rev. B* **2016**, *93*, 235305; b) W. Water, T. H. Fang, Y. J. Hsiao, L. W. Ji, J. H. Tsai, C. C. Lee, *Nanosci. Nanotechnol. Lett.* **2011**, *3*, 468–471.
[9] a) A. A. M. Sakib, S. M. Masum, J. Hoinkis, R. Islam, M. A. I. Molla, *J. Compos. Sci.* **2019**, *3*, 91; b) C. Fan, F. Sun, X. Wang, M. Majidi, Z. Huang, P. Kumar, B. Liu, *J. Mater. Sci.* **2020**, *55*, 7702–7714; c) H. Güney, D. İskenderoğlu, M. E. Güldüren, K. Ç. Dem\i˙r, S. M. Karadeniz, *Opt. Mater. (N. Y.)* **2022**, *132*, 112869.
[10] a) M. T. Thein, S.-Y. Pung, A. Aziz, M. Itoh, *J. Exp. Nanosci.* **2015**, *10*, 1068–1081; b) M. S. Abdel-wahab, A. Jilani, A. Alshahrie, A. H. Hammad, *J. Mater. Sci. Mater. Electron.* **2018**, *29*, 3056–3065; c) G. Kasi, K. Viswanathan, K. Sadeghi, J. Seo, *Prog. Org. Coat.* **2019**, *133*, 309–315.
[11] a) D. Naveena, R. Dhanabal, A. Chandra Bose, *Opt. Mater.* **2022**, *127*, 112266; b) T. Gnanasekar, S. Valanarasu, M. Ubaidullah, M. Alam, A. Nafady, P. Mohanraj, I. L. Poul Raj, T. Ahmad, M. Shahazad, B. Pandit, *Opt. Mater.* **2022**, *123*, 111954; c) R. Panda, M. Patel, J. Thomas, H. C. Joshi, *Thin Solid Films* **2022**, *744*, 139080.
[12] a) Z. N. Kayani, Z. Bashir, S. Riaz, S. Naseem, Z. Saddiqe, *J. Mater. Sci. Mater. Electron.* **2020**, *31*, 11911–11926; b) T. Gnanasekar, S. Valanarasu, H. T. Das, N. Chidhambaram, R. S. Rimal Isaac, A. M. Al-Enizi, M. Ubaidullah, V. R. M. Reddy, *J. Mater. Sci. Mater. Electron.* **2022**, *33*, 18786–18797; c) D. Jung, S. Hwang, H.-J. Kim, J.-H. Han, H.-N. Lee, *Materials* **2022**, *15*, 7270; d) N. Jhansi, D. Balasubramanian, J.-H. Chang, K. Mohanraj, R. Marnadu, M. A. Manthrammel, M. Shkir, *Silicon* **2022**, *14*, 8193–8203.
[13] a) S. M. Muzaffar, S. Naeem, S. Yaseen, S. Riaz, Z. N. Kayani, S. Naseem, *J. Sol-Gel Sci. Technol.* **2020**, *95*, 88–100; b) L. Y. Li, Y. H. Cheng, X. G. Luo, H. Liu, G. H. Wen, R. K. Zheng, S. P. Ringer, *Nanotechnology* **2010**, *21*, 145705; c) V. Ramya, K. Neyvasagam, R. Chandramohan, S. Valanarasu, A. M. F. Benial, *J. Mater. Sci. Mater. Electron.* **2015**, *26*, 8489–8496; d) X. Hu, F. Gao, Y. Xiang, H. Wu, X. Zheng, J. Jiang, J. Li, H. Yang, S. Liu, *Mater. Lett.* **2016**, *176*, 282–284; e) H. Safdar, R. Aydın, B. Şahin, *Ceram. Int.* **2022**, *48*, 26678–26688.
[14] a) B. Şahin, R. Aydin, S. Soylu, M. Türkmen, M. Kara, A. Akkaya, H. Çetin, E. Ayyıldız, *Inorg. Chem. Commun.* **2022**, *135*, 109088; b) P. P. Bagwade, D. B. Malavekar, S. B. Ubale, R. N. Bulakhe, I. In, U. M. Patil, C. D. Lokhande, *Electrochim. Acta* **2022**, *408*, 139933.
[15] a) A. Srivastava, S. Jit, S. Tripathi, *IEEE Electron Device Lett.* **2021**, *42*, 1802–1805; b) M. Poloju, N. Jayababu, M. V. Ramana Reddy, *Mater. Sci. Eng. B* **2018**, *227*, 61–67; c) S. M. Yakout, A. M. El-Sayed, *Adv. Powder Technol.* **2019**, *30*, 2841–2850; d) S. Rahemi Ardekani, A. Sabour Rouhaghdam, M. Nazari, *Chem. Phys. Lett.* **2018**, *705*, 19–22; e) B. Şahin, G. Ozyilmaz, T. Kaya, *Mater. Today Chem.* **2023**, *29*, 101448.
[16] a) Y. Liu, C. Chu, Y. Li, P. Deng, Y. Liu, R. Wu, X. Liu, Y. Zheng, W. Zhang, J. Wu, H. Li, Z. Kang, *J. Alloys Compd.* **2022**, *914*, 165258; b) K. R. Gbashi, A. A. Najim, M. A. H. Muhi, A. T. Salih, *Plasmonics* **2019**, *14*, 623–630; c) J. Kazmi, P. C. Ooi, B. T. Goh, M. K. Lee, M. F. M. Razip Wee, S. Shafura, A. Karim, S. R. Ali Raza, M. A. Mohamed, *RSC Adv.* **2020**, *10*, 23297–23311; d) Y. Nie, Y. Xie, Y. Zheng, Y. Luo, J. Zhang, Z. Yi, F. Zheng, L. Liu, X. Chen, P. Cai, P. Wu, *Coating* **2021**, *11*, 1140; e) K. Sedeek, E. Abdeltwab, H. Hantour, N. Makram, *J. Supercond. Novel Magn.* **2020**, *33*, 445–453.
[17] a) B. Şahin, R. Aydın, H. Çetin, *Ceram. Int.* **2019**, *45*, 16748–16758; b) P. Scherrer, *Ges Wiss Göttingen* **1918**, *26*, 98–100.
[18] a) B. D. Cullity, S. R. Stock, *Elements of x-ray diffraction*, 3rd ed., Prentice Hall, Upper Saddle River, NJ, **2001**, p. 664; b) Z. Braiek, M. Gannouni, I. Ben Assaker, A. Bardaoui, A. Lamouchi, A. Brayek, R. Chtourou, *Eur. Phys. J. Appl. Phys.* **2015**, *72*, 10302.
[19] a) P. P. Sahay, R. K. Nath, *Sens. Actuators B* **2008**, *134*, 654–659; b) A. Augustin, K. R. Udupa, B. K. Udaya, *AIP Conf. Proc.* **2016**, *1728*, 020492.
[20] N. Sadananda Kumar, K. V. Bangera, C. Anandan, G. K. Shivakumar, *J. Alloys Compd.* **2013**, *578*, 613–619.
[21] a) N. Sedefoğlu, H. Kavak, *SDU Fen Edb. Fak. Fen Dergisi* **2021**, *16*, 147–156; b) Z. Wang, Z. Niu, Q. Hao, L. Ban, H. Li, Y. Zhao, Z. Jiang, *Catalysts* **2019**, *9*, 35.
[22] E. Gürbüz, B. Şahin, *Appl. Phys. A Mater. Sci. Process.* **2018**, *124*, 795.
[23] S. Das, V. C. Srivastava, *J. Nano Res.* **2015**, *35*, 21–26.
[24] a) S. Azhar, K. S. Ahmad, I. Abrahams, W. Lin, R. K. Gupta, M. Mazhar, D. Ali, *RSC Adv.* **2021**, *11*, 30510–30519; b) M. Rajasekaran, P. Kumaresan, S. Nithiyanantham, V. K. Subramanian, S. Kalpana, *Chem. Afr.* **2022**, *5*, 89–97.
[25] B. Şahin, R. Aydin, H. Cetin, *Superlattices Microstruct.* **2020**, *143*, 106546.
[26] a) Y. Yulizar, R. Bakri, D. O. B. Apriandanu, T. Hidayat, *Nano-Struct. Nano-Objects* **2018**, *16*, 300–305; b) B. Şahin, A. Acar, T. Kaya, *Ceram. Int.* **2021**, *47*, 11405–11414.
[27] a) A. K. Sahoo, M. R. Panigrahi, *Results Chem.* **2022**, *4*, 100614; b) H. J. Jung, S. Park, K. D. Kim, T. H. Kim, M. Y. Choi, K. Y. Lee, *Colloids Surf. A* **2018**, *550*, 37–45.
[28] a) E. Muchuweni, T. S. Sathiaraj, H. Nyakotyo, *Ceram. Int.* **2016**, *42*, 10066–10070; b) M. Thirumoorthi, J. T. J. Prakash, *J. Asian Ceram. Soc.* **2016**, *4*, 39–45.
[29] G. Sungi, M. E. Samiji, N. R. Mlyuka, E. T. Shana, *J. Mater. Sci. Mater. Electron.* **2023**, *34*, 768.
[30] S. Yu, L. Li, Z. Sun, H. Zheng, H. Dong, D. Xu, W. Zhang, *J. Am. Ceram. Soc.* **2015**, *98*, 1121–1127.
[31] a) A. Akkaya, B. Şahin, R. Aydın, H. Çetin, E. Ayyıldız, *J. Mater. Sci. Mater. Electron.* **2020**, *31*, 14400–14410; b) N. S. Kirik, B. Şahin, *Micro Nanostr.* **2022**, *167*, 207290.
[32] a) J. F. Xu, W. Ji, Z. X. Shen, W. S. Li, S. H. Tang, X. R. Ye, D. Z. Jia, X. Q. Xin, *J. Raman Spectrosc.* **1999**, *30*, 413–415; b) A.-J. Cheng, Y. Tzeng, H. Xu, S. Alur, Y. Wang, M. Park, T.-h. Wu, C. Shannon, D.-J. Kim, D. Wang, *J. Appl. Phys.* **2009**, *105*, 073104.
[33] a) P. Brüesch, *Phonons: Theory and Experiments I: Lattice Dynamics and Models of Interatomic Forces*, Springer Berlin Heidelberg, Berlin, **1982**, p. 273; b) M. F. N. Taufique, A. Haque, P. Karnati, K. Ghosh, *J. Electron. Mater.* **2018**, *47*, 6731–6745.
[34] T. C. Damen, S. P. S. Porto, B. Tell, *Phys. Rev.* **1966**, *142*, 570–574.
[35] a) L. Bergman, X.-B. Chen, J. Huso, J. L. Morrison, H. Hoeck, *J. Appl. Phys.* **2005**, *98*, 093507; b) R. Udayabhaskar, B. Karthikeyan, *J. Appl. Phys.* **2014**, *115*, 154303.
[36] A. Sahai, N. Goswami, *Phys. E (Amsterdam, Neth.)* **2014**, *58*, 130–137.
[37] a) K. N. Tonny, R. Rafique, A. Sharmin, M. S. Bashar, Z. H. Mahmood, *AIP Adv.* **2018**, *8*, 065307; b) D. K. Schroder, *Semiconductor Material And Device Characterization*, John Wiley & Sons, New York, **2006**, p.1–59.
[38] a) J. Kang, G. Jo, J.-H. Ji, J.-H. Koh, *Ceram. Int.* **2019**, *45*, 23934–23940; b) R. Aydın, A. Akkaya, B. Şahin, *J. Mater. Sci. Mater. Electron.* **2022**, *33*, 23806–23820.
[39] O. Kahveci, A. Akkaya, R. Aydın, B. Şahin, E. Ayyıldız, *Inorg. Chem. Commun.* **2023**, *147*, 110230.
[40] a) O. Daoudi, A. Elmadani, M. Lharch, M. Fahoume, *Opt. Quantum Electron.* **2020**, *52*, 413; b) A. Akkaya, O. Kahveci, R. Aydın, B. Şahin, *Appl. Phys. A Mater. Sci. Process.* **2021**, *127*, 911.
[41] H. N. Sheikh, H. Khajuria, J. Ladol, R. Singh, *Acta Chim. Slov.* **2015**, *62*, 849–858.
[42] Y. Altinay, E. Gökoğlan, Ç. Yener, G. Ünlü, B. Şahin, *Appl. Phys. A Mater. Sci. Process.* **2022**, *128*, 784.

Manuscript received: May 11, 2023
Revised manuscript received: July 14, 2023
Version of record online: August 3, 2023